

# Crimean–Congo hemorrhagic fever virus nucleoprotein reveals endonuclease activity in bunyaviruses

Yu Guo<sup>a,b,c,1</sup>, Wenming Wang<sup>b,c,1</sup>, Wei Ji<sup>b,c</sup>, Maping Deng<sup>d</sup>, Yuna Sun<sup>e</sup>, Honggang Zhou<sup>b,c</sup>, Cheng Yang<sup>b,c</sup>, Fei Deng<sup>d</sup>, Hualin Wang<sup>d</sup>, Zhihong Hu<sup>d,2</sup>, Zhiyong Lou<sup>a,2</sup>, and Zihe Rao<sup>a,b,c,e,2</sup>

<sup>a</sup>Laboratory of Structural Biology and Ministry of Education (MOE) Laboratory of Protein Science, School of Medicine and Life Sciences, Tsinghua University, Beijing 100084, China; <sup>b</sup>College of Life Sciences and Pharmacy, Nankai University, Tianjin 300071, China; <sup>c</sup>State Key Laboratory of Virology, Wuhan Institute of Virology, Chinese Academy of Sciences, Wuhan 430071, China; <sup>d</sup>High-Throughput Molecular Drug Discovery Center, Tianjin Joint Academy of Biomedicine and Technology, Tianjin 300457, China; and <sup>e</sup>National Laboratory of Macromolecules, Institute of Biophysics, Chinese Academy of Science, Beijing 100101, China

Edited by Peter Palese, Mount Sinai School of Medicine, New York, NY, and approved February 21, 2012 (received for review January 17, 2012)

Crimean–Congo hemorrhagic fever virus (CCHFV), a virus with high mortality in humans, is a member of the genus *Nairovirus* in the family *Bunyaviridae*, and is a causative agent of severe hemorrhagic fever (HF). It is classified as a biosafety level 4 pathogen and a potential bioterrorism agent due to its aerosol infectivity and its ability to cause HF outbreaks with high case fatality (~30%). However, little is known about the structural features and function of nucleoproteins (NPs) in the *Bunyaviridae*, especially in CCHFV. Here we report a 2.3-Å resolution crystal structure of the CCHFV nucleoprotein. The protein has a racket-shaped overall structure with distinct “head” and “stalk” domains and differs significantly with NPs reported so far from other negative-sense single-stranded RNA viruses. Furthermore, CCHFV NP shows a distinct metal-dependent DNA-specific endonuclease activity. Single residue mutations in the predicted active site resulted in a significant reduction in the observed endonuclease activity. Our results present a new folding mechanism and function for a negative-strand RNA virus nucleoprotein, extend our structural insight into bunyavirus NPs, and provide a potential target for antiviral drug development to treat CCHFV infection.

structure biology | virology

Crimean–Congo hemorrhagic fever virus (CCHFV) is a tick-borne virus and the causative agent of Crimean–Congo hemorrhagic fever (CCHF), a severe human disease that occurs in over 30 countries in Asia, the Middle East, Southeastern Europe, and Africa (1, 2) and results in high mortality. There is currently no vaccine against CCHF and available therapeutic interventions are limited. The high pathogenicity of CCHFV has led to it being considered as a severe public health threat and a potential bioterrorism agent in the wider world. It is therefore classified as a World Health Organization biosafety level 4 pathogen, limiting fundamental investigations in the laboratory (2).

CCHFV is a negative-sense single-stranded RNA [(–)ssRNA] virus with a three-segmented genome and belongs to the genus *Nairovirus* within the family *Bunyaviridae* (2). The *Bunyaviridae* is the largest negative-sense viral family and comprises more than 350 species, including many significant human pathogens, such as Rift Valley fever, Crimean–Congo hemorrhagic fever, hanta, and sandfly fever viruses. The bunyavirus genomes consist of small (S), medium (M), and large (L) RNA segments, which encode a viral nucleocapsid protein (NP), glycoprotein precursor, and polymerase proteins, respectively (3). According to previous studies on the function of nucleoproteins in bunyaviruses, some of these NPs may be able to recognize specific viral RNA sequences (4–6), but mostly bind to single-stranded RNA (ssRNA) in a nonspecific way (7, 8). Because the *Bunyaviridae* family includes hundreds of different genera and the nucleoproteins of each genus show little homology or other features in common, the addressing of the exact function and mechanism of each group of nucleoproteins case by case is necessary for our understanding on bunyaviruses replication and assembly. To our knowledge, the only NP structure reported to date in the *Bunyaviridae* family is the Rift Valley fever virus nucleoprotein (9, 10), which shows weak binding affinity with RNA and displays a conformational change before

oligomerization into a ribonucleoprotein (RNP) complex (9). Previous structures of NPs from other families, such as the influenza virus (*Orthomyxoviridae*) (11, 12), rabies virus (*Rhabdoviridae*) (13), vesicular stomatitis virus (VSV) (*Rhabdoviridae*) (14), and borna disease virus (BDV) (*Bornaviridae*) (15) have shown how NPs assemble with RNA to form RNPs. Interestingly, recent studies by two research groups on the structure of the Lassa fever virus (LASV) (*Arenaviridae*) NP have added to our understanding of the functions of virally encoded NPs beyond their role in the packaging of viral genomic RNA (16–18). Both groups concur that the LASV C-terminal domain possesses 3′–5′ RNA-specific exoribonuclease activity, whereas they hold different opinions on the function of the N-terminal domain. Qi et al. describe a LASV NP(1-569)-dTTP complex structure and propose that the LASV NP is responsible for the RNA cap-snatching mechanism that initiates its transcription (18). In contrast, Hastie and colleagues report the structure of a LASV(1-340)-ssRNA complex showing that the N-terminal domain possesses an RNA-binding crevice for the viral genome (17). Bearing in mind the potential relationship between the two negative single-strand RNA viruses CCHFV and LASV, and our lack of knowledge of the biological role and precise mechanisms of NPs in the bunyaviruses, we conducted a structural and biochemical analysis of CCHFV NP.

## Results

**CCHFV NP Exists as a Monomer in Vitro.** The full-length CCHFV NP protein (strain YL04057) was expressed and purified as a recombinant protein in *Escherichia coli*. As oligomerization of NPs has been observed in several (–)ssRNA viruses (9, 11, 12, 19), we first determined the oligomeric state of CCHFV NP. Gel filtration and SDS–PAGE showed that CCHFV NP mainly exists in a monomeric form with DNase/RNase treatment (Fig. 1), which differs from other reported (–)ssRNA viruses except for Rift Valley fever virus (RFV) NP in its compact conformation (10).

**Overall Structure of CCHFV NP.** The crystal structure of monomeric CCHFV NP (residues 1–482) was determined using the single-wavelength anomalous dispersion (SAD) method and refined to 2.3 Å resolution with a final  $R_{\text{work}}$  value of 22.4% ( $R_{\text{free}} = 25.7\%$ ) (Table 1). The final model contains the full-length polypeptide, except for residues L181–S194 and S367–N371,

Author contributions: Y.G., F.D., H.W., Z.H., Z.L., and Z.R. designed research; Y.G., W.W., W.J., M.D., Y.S., and H.Z. performed research; M.D., F.D., and H.W. contributed new reagents/analytic tools; Y.G., Y.S., H.Z., C.Y., F.D., H.W., Z.H., Z.L., and Z.R. analyzed data; and C.Y., Z.H., Z.L., and Z.R. wrote the paper.

The authors declare no conflict of interest.

This article is a PNAS Direct Submission.

Data deposition: The atomic coordinate and structure factor have been deposited in the Protein Data Bank ([www.rcsb.org](http://www.rcsb.org)) with the accession code 3U3I.

<sup>1</sup>Y.G. and W.W. contributed equally to this work.

<sup>2</sup>To whom correspondence may be addressed: E-mail: raozh@xtal.tsinghua.edu.cn, louzy@xtal.tsinghua.edu.cn, or huzh@wh.iov.cn.

This article contains supporting information online at [www.pnas.org/lookup/suppl/doi:10.1073/pnas.1200808109/-DCSupplemental](http://www.pnas.org/lookup/suppl/doi:10.1073/pnas.1200808109/-DCSupplemental).

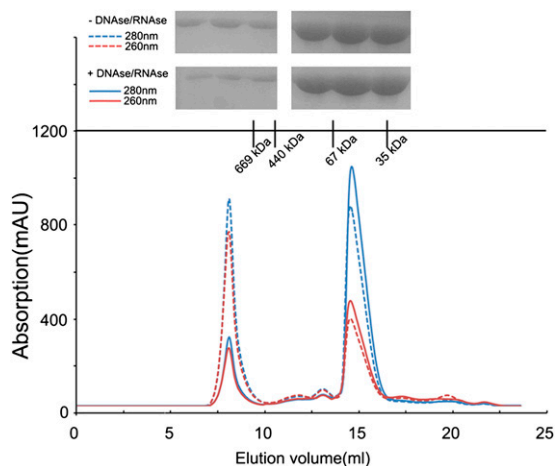


**Fig. 1.** Size exclusion chromatography (SEC) of CCHFV NP. CCHFV NP samples with or without DNase/RNase treatment (5 mg/mL) were injected, respectively, onto a Superdex 200 10/300 GL column. Retention volume was about 15 mL for the monomeric form of CCHFV NP. (Upper) Retention volumes are shown for the molecular weight standards and SDS/PAGE analysis of the SEC elution fractions corresponding to the two peaks.

which could not be built due to a lack of interpretable electron density, indicating their high structural flexibility.

CCHFV NP possesses a racket-shaped overall structure with dimensions of  $40 \times 50 \times 95 \text{ \AA}$ , and features two major parts: a “head” domain (M1-I180 and A300-I482) and a “stalk” domain (R181-A299) (Fig. 2). Both head and stalk domains are predominantly composed of  $\alpha$ -helices. There is a large positively charged cavity located at the center of the head domain, and a positively

charged region in the stalk domain adjacent to the head domain (Fig. 3). Although CCHFV NP has no primary sequence homologs, a comparison of the structure of the head domain with reported structures in the Protein Data Bank (PDB) using the DALI structure comparison service (20) revealed a high structural similarity with the N-terminal domain of LASV NP (18) (PDB code: 3MX5, Z score = 15.5). Alignment of these two structures gives an overall root-mean-square deviation (rmsd) of 3.2  $\text{\AA}$  for all C $\alpha$  atoms of the 259 aligned residues (Fig. S1).

LASV belongs to the *Arenaviridae* family and is a single-stranded ambisense RNA virus with two genomic RNA segments encoding four genes, and its NP is responsible for encapsulating the viral genomic RNA into ribonucleoprotein (21). Qi and colleagues presented the first full-length LASV NP structure and proposed that the full-length LASV NP contains an RNA-specific 3'-5' exonuclease activity (18). This exonuclease activity was confirmed by an independent group who located this function to the C-terminal domain (16). However, Qi et al. also suggested that the N-terminal domain of LASV NP contains an RNA cap-binding function, whereas a newly reported LASV(1-340)-ssRNA complex structure shows that the N-terminal domain actually possesses RNA-binding activity (17). The CCHFV NP head domain shows high structural similarity with the LASV NP N-terminal domain, despite poor primary sequence similarity (Fig. S1).

**Cap-Binding Ability of CCHFV NP.** Because the CCHFV NP head domain shows high structural similarity to the LASV NP N-terminal domain, we first investigated whether they have similar functions. We first examined the cap-binding ability of the CCHFV NP head domain. Results of isothermal titration calorimetry showed, unexpectedly, that the monomeric CCHFV NP binds cap analogs, i.e., m7G, m7Gp, and m7Gppp, with extremely low or no binding affinity in vitro (Fig. S2), compared with the cap-binding affinities reported for bona fide virally encoded cap-binding proteins (22). Attempts to cocrystallize or soak crystals of CCHFV NP with cap analogs were also carried out, but no extra

**Table 1. Data collection and refinement statistics**

Parameters	Native	Selenomethionine peak
Data collection statistics		
Cell parameters		
<i>a</i>	58.3	57.1
<i>b</i>	67.9	68.2
<i>c</i>	131.5	131.1
$\alpha, \beta, \gamma$ ( $^\circ$ )	90.0, 90.0, 90.0	90.0, 90.0, 90.0
Space group	$P2_12_12_1$	$P2_12_12_1$
Wavelength used, $\text{\AA}$	1.0000	0.9798
Resolution, $\text{\AA}$	50.00–2.30 (2.34–2.30) <sup>†</sup>	50.00–3.10 (3.15–3.10)
No. of all reflections	155,036 (8,610)	89,319 (6,840)
No. of unique reflections	22,556 (1,196)	12,908 (980)
Completeness (%)	99.1 (99.7)	99.9 (100.0)
Average $I/\sigma(I)$	13.5 (4.9)	9.0 (6.1)
$R_{\text{merge}}$ (%) <sup>*</sup>	6.1 (36.2)	10.2 (41.9)
Refinement statistics		
No. of reflections used ( $\sigma(F) > 0$ )		21,212
$R_{\text{work}}$ (%) <sup>†</sup>		22.4
$R_{\text{free}}$ (%) <sup>†</sup>		25.7
rmsd bond distance, $\text{\AA}$		0.025
rmsd bond angle, $^\circ$		2.461
Average <i>B</i> value, $\text{\AA}^2$		37.4
Ramachandran plot		
Res. in favored regions, %		93.0
Res. in generously allowed regions, %		3.1
Res. in disallowed regions, %		2.9

<sup>\*</sup> $R_{\text{merge}} = \sum_h \sum_i |I_{ih} - \langle I_h \rangle| / \sum_h \sum_i \langle I_h \rangle$ , where  $\langle I_h \rangle$  is the mean of the observations  $I_{ih}$  of reflection  $h$ .

<sup>†</sup> $R_{\text{work}} = \sum (|F_o(\text{obs}) - F_p(\text{calc})|) / \sum F_o(\text{obs})$ ;  $R_{\text{free}}$  is an *R* factor for a preselected subset (5%) of reflections that was not included in refinement.

<sup>‡</sup>Numbers in parentheses are corresponding values for the highest resolution shell.

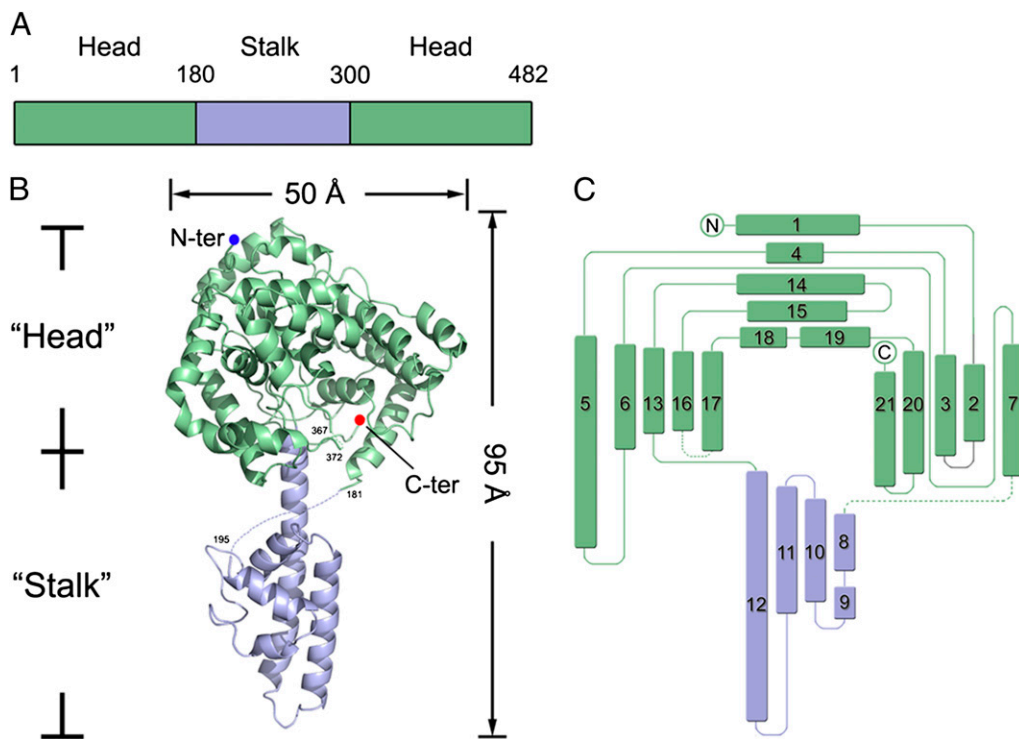


**Fig. 2.** Structure of CCHFV NP. (A) Schematic diagram of the domain organization in the primary sequence of CCHFV NP. The stalk and head domains are colored as light blue and green, respectively. (B) Overall structure in cartoon representation. Missing residues are linked by dotted lines. (C) Topology diagram. Head and stalk domains are colored in green and light blue, respectively.

electron density was observed in the potential cap-binding site suggested by structural comparisons with LASV NP. We therefore conclude that CCHFV NP, at least in its monomeric form, is unlikely to bind with the cap *in vitro*.

**RNA-Binding Affinity of CCHFV NP.** We subsequently examined whether CCHFV NP binds RNA at a range of different concentrations using electrophoretic mobility shift assays (EMSAs) (Fig. S3) and found that CCHFV NP's binding affinity with a 24-nt ssRNA probe was weak, because free RNA could still be observed even at a NP:RNA molar ratio of 16:1. Surface plasmon resonance spectroscopy analysis also revealed poor binding affinity with a poly (U) oligonucleotide (Fig. S4). These results are consistent with the weak nucleic acid-binding affinity observed during purification (Fig. 1). When treated with DNase and RNase (1  $\mu\text{g}/\text{mL}$ ), CCHFV NP could easily be separated from *E. coli* nucleic acids, suggesting that the binding affinity of CCHFV NP for nucleic acids is weak.

**CCHFV NP and Host Defense Mechanism.** Both CCHFV and LASV antagonize the host IFN response to infection by interfering with the activation pathway of IRF-3 (23). Further studies have suggested that, in LASV, the exoribonuclease activity encoded by the C-terminal domain of LASV NP is responsible for this sup-

pression of innate immunity (16, 18). However, results from IFN induction reporter assays driven by INF- $\beta$  or IFN-stimulated response element (ISRE) promoters indicated that CCHFV NP did not induce a significant type I IFN response (Fig. S5), suggesting that CCHFV NP may not be responsible for interruptions of the IRF-3 pathway.

Moreover, previous research has demonstrated host cell caspase-3-dependent proteolysis of CCHFV NP into two fragments when caspase activity is induced during infection and this has been proposed as a host defense mechanism against CCHFV infection (24). We confirmed this observation when purified caspase-3 was added to CCHFV NP protein *in vitro* (Fig. S6B). The cleavage site of caspase-3 on CCHFV NP was identified to be  $^{266}\text{DEVD}^{269}$  and is located in a loop region connecting two long central helices in the stalk domain (Fig. S6A). We therefore propose that host cell defenses against CCHFV infection may recognize the stalk domain of NP and thus antagonize the biological function of NP.

**CCHFV Nucleoprotein Has Endonuclease Activity.** The inconsistency between the biological functions of CCHFV NP and its structural homolog, LASV NP, led us to further investigate the biological function of CCHFV NP. Results showed that CCHFV NP has a divalent cation-dependent endonuclease activity *in vitro* (Fig. 4).

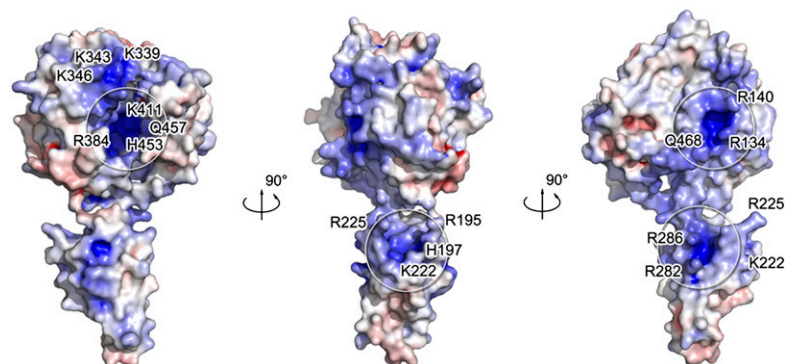


**Fig. 3.** Potential RNA-binding region of CCHFV. The electrostatic surface potential of CCHFV NP was calculated using adaptive Poisson-Boltzmann solver (APBS) tools. The positive surface is colored blue, the negative surface, red, with limits  $\pm 10$  kT/ec. Positive residues are labeled on CCHFV NP, suggesting the presence of several positively charged grooves that may be involved in RNA binding.

We assayed the nuclease activity of the CCHFV NP using ss/dsDNA (Fig. 4A) and ss/dsRNA substrates (Fig. 4B) with or without secondary structure. Using 179-nt dsDNA and ssDNA, we found that CCHFV NP has an intrinsic nuclease activity on both single- and double-stranded DNA that is stimulated to different extents by divalent cations such as  $Mn^{2+}$ ,  $Co^{2+}$ , and  $Mg^{2+}$ . Other divalent cations had little or no effect on CCHFV NP nuclease activity (Fig. 4C). In contrast, purified NP did not hydrolyze ssRNA or dsRNA in the presence or absence of  $Mn^{2+}$ , suggesting that the nuclease activity of CCHFV NP is DNA specific (Fig. 4B). CCHFV NP also completely degraded circular dsDNA and highly structured dsDNA ( $\lambda$ -DNA), showing that it is a sequence nonspecific endonuclease (Fig. 4D and Fig. S7A).

Because the head domain shows little structural similarity with other endonucleases, we carried out further experiments to confirm the above findings. We selected several residues, i.e., Y374, R384, E387, K411, H453, and Q457, which appear to be potentially involved in the putative active site, for mutational analysis (Fig. 5B). Results of *in vitro* endonuclease assays with site-specific mutants R384A, E387A, K411A, H453A, and Q457A revealed that they had significant, but different degrees of impact, whereas Y374A had only marginal effects (Fig. 5C). Not surprisingly, these positions are absolutely conserved in related NP sequences (Fig. S8). Because the only pocket within the whole protein large enough for substrate binding is located in the head domain, we wondered whether the stalk domain plays any role in

this endonuclease activity. We generated a construct (NP $_{\Delta 180-300}$ ) of the head domain in which stalk domain residues were replaced by a flexible linker consisting of glycine residues. The head domain alone showed equivalent endonuclease activity to the wild-type protein (Fig. S9), indicating that the head domain is responsible for the endonuclease activity of CCHFV NP.

In addition, we measured the specific activity of CCHFV NP. CCHFV NP showed DNA endonuclease activity as high as  $1.3 \times 10^5$  units/mg (Fig. S7B). Considering the molecular weight difference between CCHFV NP (56 kDa) and DNase I (31 kDa), this specific activity is comparable with that of a typical DNA nuclease. Taken together, all these results reveal that CCHFV NP possesses a unique endonuclease activity.

## Discussion

Our work reveals that bunyavirus nucleoprotein has an endonuclease function not present in other negative single-stranded RNA viruses. Interestingly, the paper by Qi and colleagues also reported that both trimeric and hexameric forms of LASV NP can degrade dsDNA, whereas they did not comment on which part of the LASV NP is responsible for this DNase activity (18). The similar enzymatic activity of the CCHFV and LASV nucleoproteins raises the possibility that the function of (-)ssRNA virus nucleoproteins is more complex than previously anticipated. Further work is needed to determine the precise role of CCHFV NP during the life cycle of CCHFV.

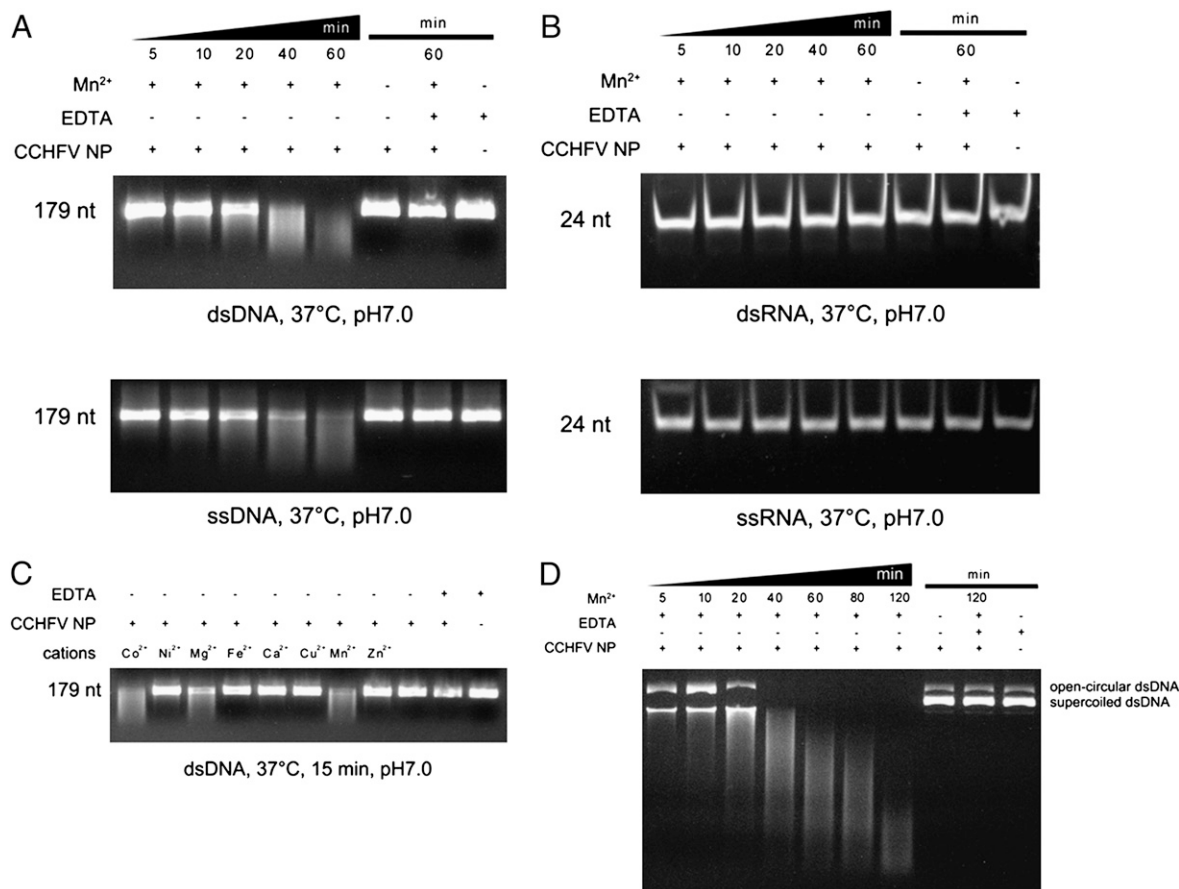


**Fig. 4.** DNA-specific endonuclease activity of CCHFV NP. (A) Time series of *in vitro* dsDNA (Upper) and ssDNA (Lower) and (B) dsRNA (Upper) and ssRNA (Lower) degradation assay products. Reaction products of 0.3  $\mu$ M purified CCHFV NP with 100 ng/ $\mu$ L substrates at 37 °C in a final volume of 10  $\mu$ L are shown after 5, 10, 20, 40, and 60 min. Reaction products were loaded onto a 20% (wt/vol) polyacrylamide gel and stained with ethidium bromide. (C) Effect of divalent cations on CCHFV NP nuclease activity. Purified CCHFV NP (0.3  $\mu$ M) and dsDNA substrate were incubated with  $CoCl_2$ ,  $NiCl_2$ ,  $MgCl_2$ ,  $FeSO_4$ ,  $CaCl_2$ ,  $CuCl_2$ ,  $MnCl_2$ , and  $ZnCl_2$  at a concentration of 1 mM. CCHFV NP alone, CCHFV NP and EDTA, or CCHFV NP and EDTA with  $Mn^{2+}$  were used as controls. All reactions were stopped by the addition of 10 mM EDTA. (D) Effect of CCHFV NP endonuclease activity on circular double-stranded plasmids. CCHFV NP was incubated with circular double-stranded plasmids for different lengths of time. All reactions were stopped by the addition of 10 mM EDTA.



Harvested cells were resuspended in lysis buffer containing 20 mM Hepes (pH 6.8), 500 mM NaCl, 1  $\mu$ g/mL DNase I, and 1  $\mu$ g/mL RNase and homogenized with a low-temperature ultra-high pressure cell disrupter (JNBIO). The lysate was centrifuged at 25,000  $\times$  g for 30 min at 4 °C to remove cell debris. The supernatant was then loaded twice onto a GST column pre-equilibrated with lysis buffer, and the GST tag was removed by digestion with PreScission protease (GE Healthcare) overnight at 4 °C. Eluted CCHFV NP protein was further purified by Superdex-200 gel filtration chromatography (GE Healthcare). SDS-PAGE analysis revealed over 95% purity of the final purified recombinant protein. The purified protein was then concentrated to 10 mg/mL in a buffer containing 20 mM Hepes (pH 6.8), 200 mM NaCl.

A CCHFV NP<sub>Δ180–300</sub> truncation was generated by overlap-extension PCR using two sets of cloning primers: 5'-CGGGATCCATGGAAAACAAATCG-3' (forward1), 5'-CCGCTCGAGTTAGATGATGTTGGC-3' (reverse1) and 5'-AGAAG-GAAGTGGGAGGAGGAGGAGGAGGTGCACAGATT-3' (forward2), 5'-CAATCT-GTGACCTCTCTCTCTCTCCCAAGTTCCTTC-3' (reverse2). We removed the stalk domain (I180-Q300) using standard molecular cloning techniques and replaced it with five glycines. This truncation product was then inserted into a pGEX-6p-1(GE Healthcare) vector using the *Bam*H1 and *Xho*I restriction sites. The protein production and purification process was the same as that for the full-length CCHFV NP protein described above.

**Crystallization.** Initial crystallization conditions were screened by the hanging drop vapor-diffusion method using Hampton Research crystal screening kits at 16 °C. Crystals were obtained by mixing 1  $\mu$ L of the protein solution with an equal volume of a reservoir solution and equilibrating the mixed drop against 300  $\mu$ L of reservoir solution.

Small crystals first appeared after 2 d in 200 mM KCl and 20% (wt/vol) PEG3350. Further optimization with additive and detergent screens (Hampton Research) was performed, and the final optimized crystals were grown in a buffer containing 20 mM KCl, 10 mM MnCl<sub>2</sub>, and 12% (wt/vol) PEG3350. Rod-like crystals grew to a final size of 20  $\times$  40  $\times$  150  $\mu$ m within 5 d. Selenomethionine substituted crystals appeared in the same condition, reaching their final size within 10 d. Crystals were harvested and cryoprotected in the well solution containing an additional 20% (vol/vol) glycerol and ash cooled in a dry nitrogen stream at 100 K for X-ray data collection.

**X-Ray Data Collection, Processing, and Structure Determination.** Diffraction data for the native crystal of CCHFV NP was first collected to 2.3 Å at 100 K using a MARResearch M165 CCD detector on beamline 1W2A at the Beijing Synchrotron Radiation Facility. Anomalous diffraction data for selenomethionine derivatives were collected to 3.1 Å at 100 K using an ADSC Q315 CCD detector on beamline BL17 at the Photon Factory (KEK, Japan). All datasets were indexed, integrated, and scaled using the HKL2000 package

(25). The orthorhombic crystal form belongs to space group *P2<sub>1</sub>2<sub>1</sub>2<sub>1</sub>* with cell parameters *a* = 58.3 Å, *b* = 67.9 Å, and *c* = 131.5 Å.

Heavy atom searching, initial phase calculations, and density modifications were performed with PHENIX (26). The resulting electron density map was displayed with COOT (27) and an initial model was built manually. Several rounds of simulated annealing, restrained individual atomic displacement parameter refinement, energy minimization, and individual B-factor refinement were carried out with PHENIX (26). Solvent molecules were located from stereochemically reasonable peaks in the  $\sigma$ A-weighted 2*F<sub>o</sub>*–*F<sub>c</sub>* difference Fourier electron density map (1.2  $\sigma$ ). Model geometry was verified using PROCHECK (28). All structure figures were drawn with PyMOL (29). Coordinates and structure factors have been deposited with the RCSB under accession code: 3U3I.

**Endonuclease Activity Assays.** The DNA cleavage assay was performed by incubating 0.3  $\mu$ M CCHFV NP with 100 ng/ $\mu$ L dsDNA or ssDNA at 37 °C in a final volume of 10  $\mu$ L. The reaction buffer was 20 mM Hepes pH 7.0, 200 mM NaCl, and 1 mM metal salts. Reactions were stopped by the addition of EDTA to a final concentration of 10 mM, and reaction products were loaded on a 1.5% agarose gel and stained with ethidium bromide. The effect of divalent cations on the DNase activity of CCHFV NP was tested by incubating DNA substrates with the protein in the presence of different metal salts: CoCl<sub>2</sub>, NiCl<sub>2</sub>, MgCl<sub>2</sub>, FeSO<sub>4</sub>, CaCl<sub>2</sub>, CuCl<sub>2</sub>, MnCl<sub>2</sub>, and ZnCl<sub>2</sub>. The circular double-stranded plasmid pGEX-6p-1 (GE Healthcare) and digested  $\lambda$ -DNA were also tested as substrates and the reaction products were loaded on a 1.5% agarose gel and stained with ethidium bromide. The reaction buffer and conditions for 24-nt RNA cleavage were the same as those for the DNA cleavage assay, and the reaction products were loaded onto 20% polyacrylamide gels and stained with ethidium bromide.

**Isothermal Titration Calorimetry.** The binding affinities of cap analogs of wild-type CCHFV NP, i.e., m<sup>7</sup>G, m<sup>7</sup>Gpp, and m<sup>7</sup>Gppp, were measured using isothermal titration calorimetry (ITC). A 0.1-mM CCHFV NP protein solution was titrated against 0.3 mM cap-analog solutions (Sigma-Aldrich) using a VP-ITC microcalorimeter (MicroCal). ITC data were collected at 25 °C and analyzed using ORIGIN (MicroCal Software).

**ACKNOWLEDGMENTS.** We thank the staff at the Beijing Synchrotron Radiation Facility and Photon Factory for their help with data collection, and Prof. Hong-bing Shu from Wuhan University who supplied the plasmids for INF induction reporter assays. This work was supported by The National Basic Research Program of China program (973 program) (no. 2010CB530100, 2010CB833602), the National Natural Science Foundation of China (no. 31000332, 31170678), and the Special Program for Key Basic Research of the Ministry of Science and Technology (no. 2007FY210700).

- Deyde VM, Khristova ML, Rollin PE, Ksiazek TG, Nichol ST (2006) Crimean-Congo hemorrhagic fever virus genomics and global diversity. *J Virol* 80:8834–8842.
- Flick R, Whitehouse CA (2005) Crimean-Congo hemorrhagic fever virus. *Curr Mol Med* 5:753–760.
- Wei PF, et al. (2010) Serial expression of the truncated fragments of the nucleocapsid protein of CCHFV and identification of the epitope region. *Viral Sin* 25:45–51.
- Ogg MMPJ, Patterson JL (2007) RNA binding domain of Jamestown Canyon virus S segment RNAs. *J Virol* 81:13754–13760.
- Osborne JCER, Elliott RM (2000) RNA binding properties of bunyamwera virus nucleocapsid protein and selective binding to an element in the 5' terminus of the negative-sense S segment. *J Virol* 74:9946–9952.
- Mir MABB, Brown B, Hjelle B, Duran WA, Panganiban AT (2006) Hantavirus N protein exhibits genus-specific recognition of the viral RNA panhandle. *J Virol* 80:11283–11292.
- Mohl BPBJ, Barr JN (2009) Investigating the specificity and stoichiometry of RNA binding by the nucleocapsid protein of Bunyamwera virus. *RNA* 15:391–399.
- Gött P, Sr., Stohwasser R, Schnitzler P, Darai G, Bautz EK (1993) RNA binding of recombinant nucleocapsid proteins of hantaviruses. *Virology* 194:332–337.
- Ferron F, et al. (2011) The hexamer structure of Rift Valley fever virus nucleoprotein suggests a mechanism for its assembly into ribonucleoprotein complexes. *PLoS Pathog* 7:e1002030.
- Raymond DD, Piper ME, Gerrard SR, Smith JL (2010) Structure of the Rift Valley fever virus nucleocapsid protein reveals another architecture for RNA encapsidation. *Proc Natl Acad Sci USA* 107:11769–11774.
- Ng AK, et al. (2008) Structure of the influenza virus A H5N1 nucleoprotein: Implications for RNA binding, oligomerization, and vaccine design. *FASEB J* 22:3638–3647.
- Ye Q, Krug RM, Tao YJ (2006) The mechanism by which influenza A virus nucleoprotein forms oligomers and binds RNA. *Nature* 444:1078–1082.
- Albertini AA, et al. (2006) Crystal structure of the rabies virus nucleoprotein-RNA complex. *Science* 313:360–363.
- Green TJ, Zhang X, Wertz GW, Luo M (2006) Structure of the vesicular stomatitis virus nucleoprotein-RNA complex. *Science* 313:357–360.
- Rudolph MG, et al. (2003) Crystal structure of the borna disease virus nucleoprotein. *Structure* 11:1219–1226.
- Hastie KM, Kimberlin CR, Zandonatti MA, MacRae IJ, Saphire EO (2011) Structure of the Lassa virus nucleoprotein reveals a dsRNA-specific 3' to 5' exonuclease activity essential for immune suppression. *Proc Natl Acad Sci USA* 108:2396–2401.
- Hastie KM, et al. (2011) Crystal structure of the Lassa virus nucleoprotein-RNA complex reveals a gating mechanism for RNA binding. *Proc Natl Acad Sci USA* 108:19365–19370.
- Qi X, et al. (2010) Cap binding and immune evasion revealed by Lassa nucleoprotein structure. *Nature* 468:779–783.
- Fu YM, Zeng DD, Huang Q, Fan CH (2010) A scaffolded DNA origami algorithm for polygon network structures and hollow three-dimensional structures. *Acta Biophys Sin* 26:750–758.
- Holm L, Rosenstrom P (2010) Dali server: Conservation mapping in 3D. *Nucleic Acids Res* 38(Web Server issue):W545–549.
- Buchmeier MJ, Peters CJ, de la Torre JC (2007) Arenaviridae: The viruses and their replication. *Fields Virology*, eds Knipe DM, Howley PM (Lippincott Williams & Wilkins, Philadelphia), 5th Ed, pp 1791–1827.
- Guilligay D, et al. (2008) The structural basis for cap binding by influenza virus polymerase subunit PB2. *Nat Struct Mol Biol* 15:500–506.
- Martinez-Sobrido L, Giannakas P, Cubitt B, Garcia-Sastre A, de la Torre JC (2007) Differential inhibition of type I interferon induction by arenavirus nucleoproteins. *J Virol* 81:12696–12703.
- Karlberg H, Tan YJ, Mirazimi A (2011) Induction of caspase activation and cleavage of the viral nucleocapsid protein in different cell types during Crimean-Congo hemorrhagic fever virus infection. *J Biol Chem* 286:3227–3234.
- Otwinowski Z, Minor W (1997) *Processing of X-ray diffraction data collected in oscillation mode. Macromolecular Crystallography, Part A, Methods in Enzymology*, eds Carter CW, Sweet RM (Academic, New York), Vol 276, pp 307–326.
- Adams PD, et al. (2002) PHENIX: Building new software for automated crystallographic structure determination. *Acta Crystallogr D Biol Crystallogr* 58:1948–1954.
- Emsley P, Cowtan K (2004) Coot: Model-building tools for molecular graphics. *Acta Crystallogr D Biol Crystallogr* 60(Pt 12 Pt 1):2126–2132.
- Laskowski R, MacArthur M, Moss D, Thornton J (1993) PROCHECK: A program to check the stereochemical quality of protein structures. *J Appl Cryst* 26:283–291.
- DeLano WL (2002) *The PyMOL Molecular Graphics System* (DeLano Scientific, San Carlos, CA).